Journal of Alloys and Compounds 521 (2012) 183–188

Contents lists available at SciVerse ScienceDirect

Journal of Alloys and Compounds

journal homepage: www.elsevier.com/locate/jallcom

# Structural, electronic structure and magnetic studies of $GdFe_{1-x}Ni_xO_3$ ($x \leq 0.5$)

Abida Bashir[a,*], M. Ikram[a], Ravi Kumar[b], P.N. Lisboa-Filho[c]

[a] Department of Physics, National Institute of Technology, Srinagar 190006, India
[b] Centre for Material Science Engineering, National Institute of Technology, Hamirpur 177005, Himachal Pradesh, India
[c] UNESP – Univ Estadual Paulista, Faculdade de Ciências, Departamento de Física, Sao Paulo, Brazil

ARTICLE INFO

*Article history:*
Received 14 October 2011
Received in revised form 17 January 2012
Accepted 18 January 2012
Available online 28 January 2012

*PACS:*
61.05.cp
61.05.cj
75.30.Wx

*Keywords:*
XRD
X-ray absorption spectroscopy
Magnetization

ABSTRACT

The structural, electronic structure and magnetic properties of Ni doped $GdFeO_3$ perovskite materials have been studied. A decreasing trend in volume with the increasing Ni concentration without any structural change is confirmed from X-ray diffraction studies. The electronic structural studies show that the competing ions within the ensemble have +3 oxidation states, which includes the Gd, Fe and Ni ions, and also confirms the octahedral symmetry of the Fe/Ni ions. The magnetic properties clearly depict that the Ni doping can tailor the phase transitions arising due to temperature/field dependence having a heavy impact on spin dynamics.



## 1. Introduction

The diverse structural, magnetic, transport and optical properties of transition-metal oxides due to their complex d-orbitals of transition metal ion and f-orbitals of rare-earth ion make these materials important from the fundamental and technological perspectives [1]. $GdFeO_3$ is an important transition metal oxide belonging to the perovskite family, exhibiting the prototype material for $GdFeO_3$ (*Pbnm* space group) family structures, which crystallizes in an orthorhombic lattice containing pseudo cubic subcells where $Gd^{3+}$ and $Fe^{3+}$ ions occupy sites at pseudocube corners and body centers [2]. The $GdFeO_3$ system is becoming the most promising candidate for the detection of gasoline in monitoring the environment [3]. This system not only is a weak ferromagnet but also possesses a ferroelectric ground state in which the striction is generated by the exchange interaction between Gd and Fe ions. This mutual controllability of electricity and magnetism, due to composite domain wall clamping of the respective domain walls for electric and magnetic orders, plays an important role in the application of multiferroics to practical devices [4]. The low-temperature thermal conductivity is found to be strongly dependent on the magnetic field. The irreversibility of heat transport coincides with that presenting the ferroelectricity, which is due to the phonon scattering by ferroelectric domain walls. This result shows an experimental feature that point to the capability of controlling the ferroelectric domain structures by magnetic field in multiferroic materials [5]. The substitution by a homovalent transition metal results in a metal-insulator (MI) transition at a critical substitution concentration, which is associated by structural transition as studied by a number of researchers [6–13]. These studies explore the Mott's criteria of MI transition dependence on critical carrier concentration. An insight that the incorporation of Ni in $GdFeO_3$ matrix can bring new interactions due to $Ni^{3+}$–O–$Ni^{3+}$ or $Fe^{3+}$–O–$Ni^{3+}$ can be studied and verified through diverse properties like structural, magnetic, or electrical behavior or electronic structure studies. These properties would depend on different parameters, like rare-earth ion and transition metal ions' radii and spin states and hybridization of O ions with the Fe/Ni/Gd ions. In this context, the Ni doped $GdFeO_3$ system in the range of ($0 \leq x \leq 0.5$) is studied to bring to light the structural, magnetic and electronic structure evolutions.

## 2. Experimental procedures

The polycrystalline bulk samples of chemical composition $GdFe_{1-x}Ni_xO_3$ ($0 \leq x \leq 0.5$) were synthesized by solid-state reaction technique. The stoichiometric amounts of high purity (99.99%) $Gd_2O_3$, FeO and NiO powders were ground into fine powder in an agate mortar. The details of the solid state reaction technique are given in Bashir et al. [12]. Powder X-ray diffraction measurements were performed using Rigaku Rotaflex X-ray diffractometer with Cu $K\alpha$ radiation at room temperature in the $2\theta$ range of 20–80°. The near edge X-ray absorption spectroscopy (NEXAFS)

* Corresponding author. Tel.: +91 9419095975; fax: +91 01942420475.
*E-mail address:* abida.nit@gmail.com (A. Bashir).

0925-8388/$ – see front matter © 2012 Elsevier B.V. All rights reserved.
doi:10.1016/j.jallcom.2012.01.121

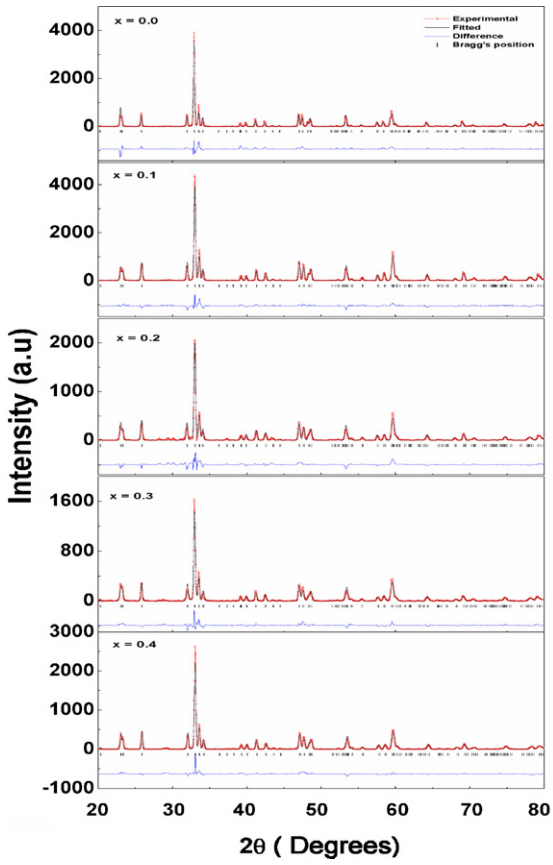


**Fig. 1.** X-ray diffraction pattern of $GdFe_{1-x}Ni_xO_3$ ($0 \le x \le 0.5$) samples.

experiments at O *K*, Fe $L_{3,2}$, Ni $L_{3,2}$, and Gd $M_{5,4}$ edges were performed at the soft X-ray beamline 7B1 XAS KIST of the Pohang Light Source (PLS), operating at 2.5 GeV with a maximum storage current of 200 mA. The spectra were collected in the total electron yield (TEY) mode and the fluorescence yield (FY) mode simultaneously at room temperature in a vacuum better than $1.5 \times 10^{-8}$ Torr. Magnetic measurements were taken in a SQUID magnetometer Quantum Design MPMS-5S (Magnetic Property Measurement System) in the temperature range of 10–350 K for applied magnetic fields up to 1 kOe. Isothermal magnetization hysteresis measurements were carried out at temperature 300 K using the VSM.

## 3. X-ray diffraction analysis

The structure of undoped $GdFeO_3$ has been reported as orthorhombic with space group *Pbnm*, which is similar to that of $RFeO_3$ as reported by Geller and Wood [14]. XRD data of $GdFe_{1-x}Ni_xO_3$ ($0.0 \le x \le 0.5$) samples exhibit single phase perovskite structure with no trace of impurity phases (e.g. $Fe_2O_3$, NiO, $Ni_2O_3$, $Gd_2O_3$ etc.), as no impurity peak is observed in the XRD spectra. The XRD patterns of samples have been refined using the Rietveld refinement method [15]. For the ease of comparison of refinement results, simulation is performed with the same initial condition as of $GdFeO_3$ with space group *Pbnm*. Fitted Rietveld refined patterns for all the samples $GdFe_{1-x}Ni_xO_3$ ($0.0 \le x \le 0.5$) are shown in Fig. 1. The observed pattern is in quite good agreement with the calculated profile with $\chi^2$ (*goodness of fit*) ~1.2. It further confirms the fact that all $GdFe_{1-x}Ni_xO_3$ samples are in single phase and correspond to the space group *Pbnm*. Calculated lattice parameters and unit cell volume for these samples is given in Table 1. It is clearly evident from the XRD analysis that there is no change in structural symmetry (orthorhombic) except the changes in lattice parameters with Ni substitution (see Table 1). Shift of peaks toward higher $2\theta$ indicates lattice contraction due to the $Ni^{3+}$ substitution at the $Fe^{3+}$ site, leading to the distortion of $Fe/NiO_6$ octahedra. It is

**Table 1**
The lattice parameters and unit cell volume for different compositions of $GdFe_{1-x}Ni_xO_3$ ($0 \le x \le 0.5$).

| Concentration | Symmetry | *a* (Å) | *b* (Å) | *c* (Å) | $V^0$ (Å$^3$) |
|---|---|---|---|---|---|
| $x = 0.0$ | Orthorhombic | 5.3464 | 5.6035 | 7.6652 | 229.6394 |
| $x = 0.1$ | Orthorhombic | 5.3350 | 5.6019 | 7.6370 | 228.2387 |
| $x = 0.2$ | Orthorhombic | 5.3343 | 5.6050 | 7.6352 | 228.2838 |
| $x = 0.3$ | Orthorhombic | 5.3425 | 5.5931 | 7.6479 | 228.5249 |
| $x = 0.4$ | Orthorhombic | 5.3341 | 5.5852 | 7.6280 | 227.2569 |
| $x = 0.5$ | Orthorhombic | 5.3212 | 5.5849 | 7.6271 | 226.6643 |

RF = 0.0582 and $Chi^2$ = 1.179.

also evident from Table 1 that parameter *a* is continuously decreasing with the increase in Ni concentration, whereas parameters *b* and *c* show small irregular variation with increasing Ni content. The overall unit cell volume is found to decrease with the increase in Ni concentration. This may be attributed to the smaller ionic radii of $Ni^{3+}$ (0.58 Å) as compared to that of $Fe^{3+}$ (0.61 Å). When the Ni content is increased beyond 0.5, new peaks tend to appear. This is due to the saturation limit of solubility of Ni in the system. These peaks correspond to the mixed phase of Ni as indexed with the Joint Committee on Powder Diffraction Standards (JCPDS) files.

## 4. X-ray absorption spectroscopy

NEXAFS and extended X-ray absorption fine structure (EXAFS) enable us to study deeply the electronic structure of the system. Owing to its simplicity and universality, the NEXAFS technique is most widely used in determining the valence states of atoms and local site symmetries in solids. The active role of the orbital degrees

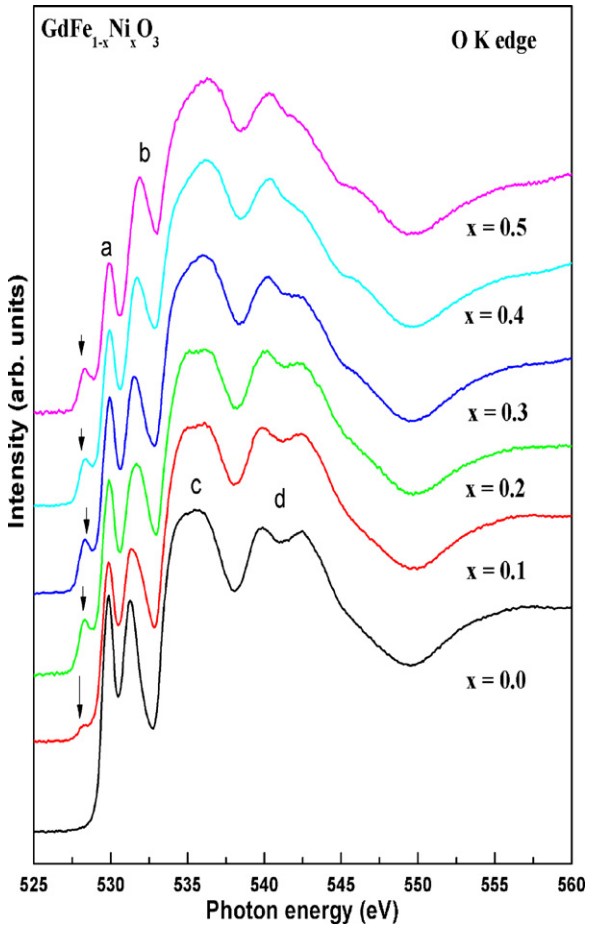


**Fig. 2.** Normalized O K edge NEXAFS spectra of $GdFe_{1-x}Ni_xO_3$ ($0 \le x \le 0.5$) samples.

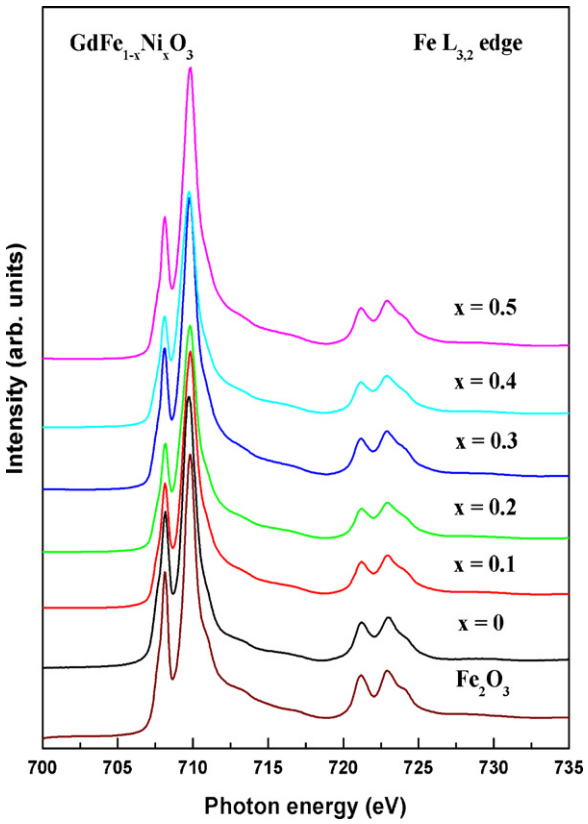


**Fig. 3.** Normalized Fe $L_{3,2}$ edge NEXAFS spectra of $GdFe_{1-x}Ni_xO_3$ ($0 \le x \le 0.5$) samples.

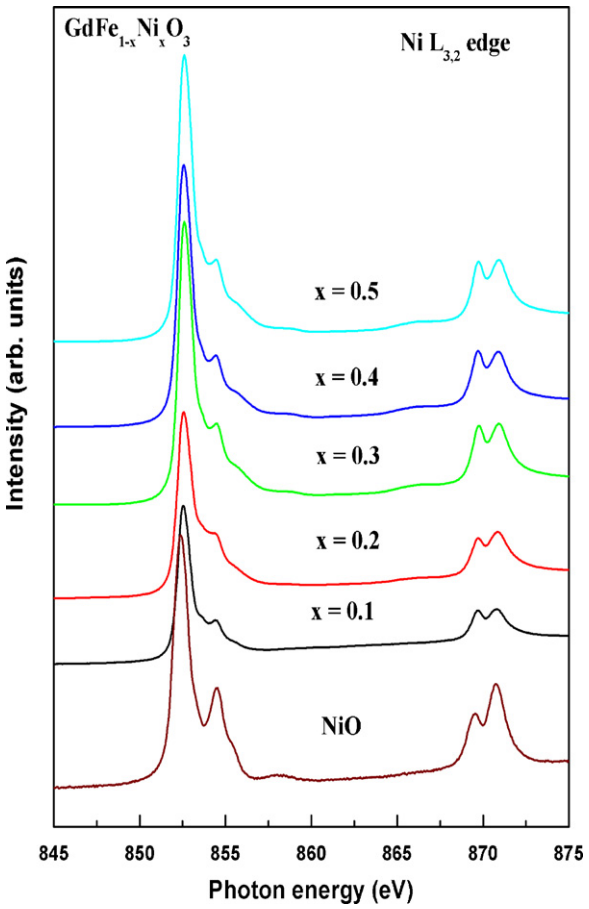


**Fig. 4.** Normalized Ni $L_{3,2}$ edge NEXAFS spectra of $GdFe_{1-x}Ni_xO_3$ ($0 \le x \le 0.5$) samples.

of freedom within its complicated perovskite structure can be typically observed in the lattice and electronic response. The electronic structure is derived from the hybridized transition metal ions' (TMI) 3d with O 2p orbitals in the structural and chemical environment of a perovskite. In this quest, we have observed the XAS studies on O *K*, Fe $L_{3,2}$, Ni $L_{3,2}$ and Gd $M_{5,4}$ edges in the given system.

The O K-edge NEXAFS spectra, representing the orbital nature of the spectral features of the O 2p unoccupied states in the conduction bands and its hybridization with different Fe and Gd orbitals, can be efficiently used to explore all kinds of possible hybridizations with different cations normalized to incident photon flux. Fig. 2 represents the normalized O K-edge NEXAFS spectra at different Ni concentrations. The spectra can be studied at different energy values starting with the pre-peak, carrying substantial information at 529 eV marked by an inverted arrow in the figure. The pre-peak structure is ascribed to $1s \rightarrow 3d$ transitions, either quadrupole-allowed or dipole-forbidden, where the latter becomes allowed due to a strong mixing of O 2p and Ni 3d states. The pre-peaks have their origin in the density of d-states of the neighboring transition metal atoms, showing the mixing of d states between different atoms, through hybridization with the oxygen p-band [16,17]. Similar pre-edge features have also been reported in the oxides, mainly in cuprates, manganites and Ni doped $SmFeO_3$ and $NdFeO_3$ [18,19]. Since this feature originates with Ni doping, it is ascribed to dipole transitions from O 1s to O 2p states that are hybridized with the unoccupied states of Ni 3d. Thus, the intensity of this peak represents the Ni 3d density of states. A continuous increase of this peak with Ni doping indicates more unoccupied states at the Ni 3d levels and hence reflects the presence of more charge carriers, electrons or holes.

The peaks marked (a) 529.92 eV and (b) 531.112 eV, where the peak separation mirrors the ligand field splitting, identified as the $t_{2g}$ and $e_g$ symmetry bands, denote the bare (ionic) crystal field splitting plus hybridization [20]. The spectral intensity shown by (c) at 537 eV and the doublet shown by (d) in the range of 539–542 eV gets merged into a single peak as the Ni concentration increases, giving clear evidence that the Ni ions are incorporated in the system and responsible for change in the electronic structure. The spectral features above 545 eV are quite similar and nearly independent of Ni concentrations, and dominated by the contribution from multiple scattering effects. This suggests that Ni ions are incorporated in the system.

$L_{2,3}$ edges have a completely different nature. The *L*-edge XANES are often of particular interest in the study of electronic properties of materials because there are three different initial states, 2s ($L_1$), $2p_{1/2}$ ($L_2$) and $2p_{3/2}$ ($L_3$), that may be coupled to final states of p, s and d character, respectively. The absorption spectrum is dominated by dipole transitions from the core 2p level to the empty 3d states, and because of the large Coulomb interaction between these two levels, it depends on the local electronic structure. Thus, it becomes mandatory to analyze the $L_{2,3}$ edges to get the information about the oxidation state and the symmetry of the 3d transition metal ions. Fig. 3 represents the NEXAFS spectra at $L_{3,2}$ of Fe in the $GdFe_{1-x}Ni_xO_3$ along with the reference compound $Fe_2O_3$. Fe 2p XAS spectra of $\alpha$-$Fe_2O_3$ and $\gamma$-$Fe_2O_3$, both formally in trivalent $Fe^{3+}$ oxides ($3d^5$) but having different local symmetries, provide full proof for the Fe in our system to be in +3 state and the symmetry is completely octahedral [21,22]. There is no change in spectral features, shifting of peaks or presence of extra peaks observed as the Ni concentration is increased, giving evidence that there is no change in valence state of Fe and its symmetry in the system due to Ni substitution [9,11].

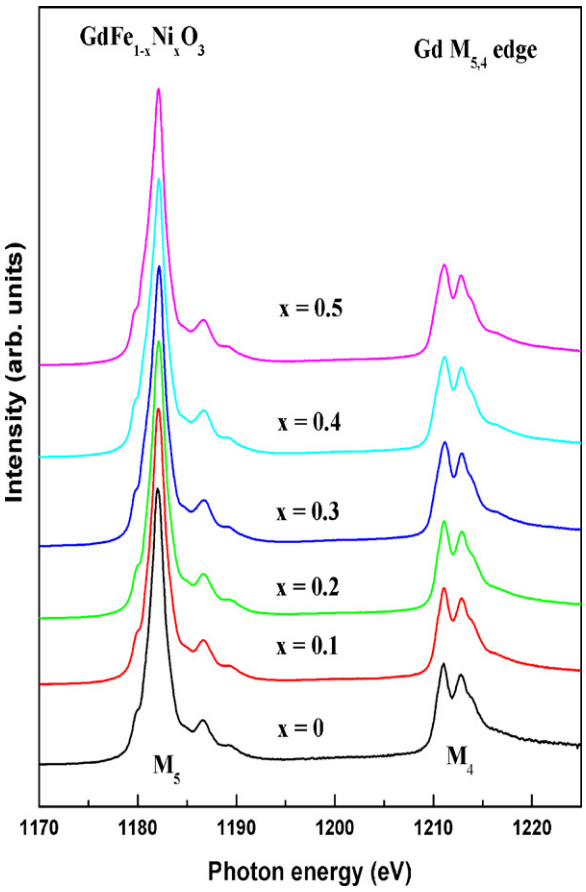


**Fig. 5.** Normalized Nd $M_{5,4}$ edge NEXAFS spectra of $GdFe_{1-x}Ni_xO_3$ ($0 \le x \le 0.5$) samples.

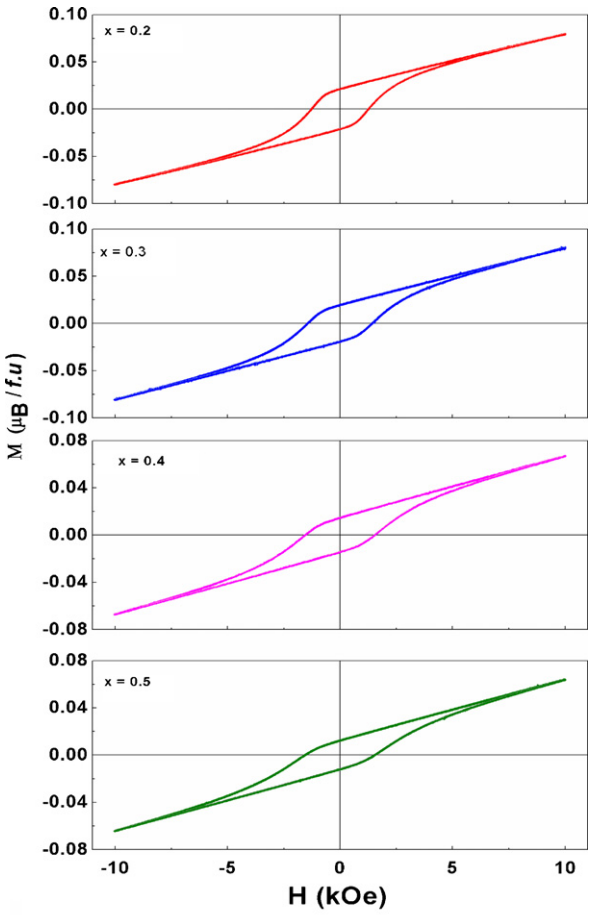


**Fig. 6.** The isothermal $M$–$H$ loops of $GdFe_{1-x}Ni_xO_3$ ($0 \le x \le 0.5$) samples at room temperature.

Fig. 4 shows the NEXAFS spectra at $L_{3,2}$ edge of Ni at room temperature for the substituted samples with the reference NiO compound. Similar to Fe $L_{3,2}$ edge, these spectra are in the form of two broad multiplet structures of $L_3$ ($2p_{3/2}$) and $L_2$ ($2p_{1/2}$), due to spin–orbit splitting of Ni 2p core holes. As per the dipole selection rules, Ni 2p electrons can be excited into empty states either with 3d or 4s symmetry. However, the intensity of 2p to 3d transition is much higher (due to higher overlap of 3d wave functions with 2p orbitals) than 2p to 4s transitions. Therefore, Ni $L_{3,2}$ edge spectra mainly probe the unoccupied states of 3d states. It is well known that the spectral feature in the case of Ni $L$-edge is highly sensitive to the spin states, which decide the unoccupancy in 3d state [23]. There is no change in spectral feature and peak positions for systems of higher Ni concentrations, which confirms the presence of $Ni^{3+}$ state in octahedral environment in these materials.

The $M_{5,4}$ edges of Gd in the $GdFe_{1-x}Ni_xO_3$ are shown in Fig. 5, which enable the quantitative valence determination of the Gd ion. Thole et al. have given the $Gd^{3+}$ plot [24]. The spectra of $Gd_2O_3$ is given by Bonnelle et al. and Kaindl et al. [25,26]. These spectra are very well matched with our Gd $M_{5,4}$ spectra, where the typical signature (i.e., peak) at 1189 eV is prominent. The XAS spectra are similar to the calculated $3d^{10}4f^7 \rightarrow 3d^9 4f^8$ spectra. These complex measured 3d absorption lines due to the $d^9 4f^{n+1}$ multiplet enable us to estimate the actual valence state of the rare earth ion, which in our case is +3. Thus, the XAS studies confirm the electronic states of the competing ions within the system.

## 5. Magnetic properties

$GdFeO_3$ is a system with paramagnetic $Gd^{3+}$ ions interacting with an antiferromagnetic system of $Fe^{3+}$ ions. The applied field H, along the crystal $a$ axis, not only has a direct spin-reorientation effect, but also increases the effect of the $Gd^{3+}$–$Fe^{3+}$ interaction, which enhances the spin reorientation effect. $GdFeO_3$ has antiferromagnetism with a Nèel point of about 2.5 K. The rapid increase of magnetization at low temperatures, i.e., below about 20 K is attributed to the slight or "parasitic" ferromagnetism in $GdFeO_3$ exhibiting pseudo perovskite characteristics and associated thermal fluctuations [27]. In $GdFeO_3$, the $Gd^{3+}$ ($^8S_{7/2}$) ions possess a spin magnetic moment giving rise to $Gd^{3+}$–$Fe^{3+}$ and $Gd^{3+}$–$Gd^{3+}$ interactions. The latter interaction causes the $Gd^{3+}$ ions to order at 1.5 K while the former are investigated in this study by their effect on the temperature dependence of the field-induced spin reorientation of the $Fe^{3+}$ ions [28].

The magnetic hysteresis loops for all the samples of $GdFe_{1-x}Ni_xO_3$ ($0.0 \le x \le 0.5$) are shown in the Fig. 6.The values for coercive field ($H_c$) for all the samples $GdFe_{1-x}Ni_xO_3$ ($0.0 \le x \le 0.5$) at 300 K are summarized in Table 2. The corresponding increased value for remnant magnetization ($M_R$) (Table 2) suggests the increase of the ferromagnetic interaction and the saturation magnetization due to incorporation of Ni. Each of these subsystems is weakly ferromagnetic due to the canting of predominantly antiferromagnetic sub lattices. The weak ferromagnetic moments of these subsystems are oriented opposite from each other, resulting in a weak ferrimagnetism. Also, the hysteresis loops are found to

**Table 2**
Parameters extracted from magnetization hysteresis at room temperature of $GdFe_{1-x}Ni_xO_3$ ($0 \le x \le 0.5$).

| Concentration | $x = 0.2$ | $x = 0.3$ | $x = 0.4$ | $x = 0.5$ |
|---|---|---|---|---|
| $H_c$ (Oe) | 1291 | 1409 | 1562 | 1604 |
| $M_R$ ($\mu_B$/fu) | 0.021 | 0.019 | 0.014 | 0.012 |
| $M$ (1T) | 0.079 | 0.080 | 0.066 | 0.063 |

be symmetrical. One plausible explanation is the coupling between spin canted structure of (weakly ferromagnetic) Fe/Ni sublattice and (antiferromagnetic) Gd sublattice.

The magnetization as a function of temperature curves, between 1 K and 300 K under ZFC and FC conditions, at the applied fields of 10 Oe, 100 Oe and 1000 Oe are given in Figs. 7–9. Similar studies have been performed on other samples (not shown due to the brevity of the manuscript). In case of the $GdFeO_3$ system, at 10 Oe the ZFC and FC lines have overlapped, indicating that there is no magnetic transition in this temperature range (1–300 K) with magnetic moment of 4.42 $\mu_B$/fu at 2 K. Similar behavior has been observed by Bedekar et al., who have studied $GdFeO_3$ system at 10 kOe showing the prominent contribution of paramagnetic contribution of the Gd system [29].

Otherwise, at 10 Oe, the system with 10, 20, 30 and 40% Ni substitution shows slight bifurcation of the ZFC and FC. Transition from the paramagnetic to antiferromagnetic phase occurs at 27.5 K, 23.5 K and 21.5 K (error of 0.5 K), having magnetic moments of 4.80, 6.80 and 3.07 $\mu_B$/fu, respectively, while there is again a phase transition at lowered temperatures at 8.46 K, 7.97 K and 9.62 K with decrement in the magnetic moment of 1.33, 4.25 and 2.27 $\mu_B$/fu,

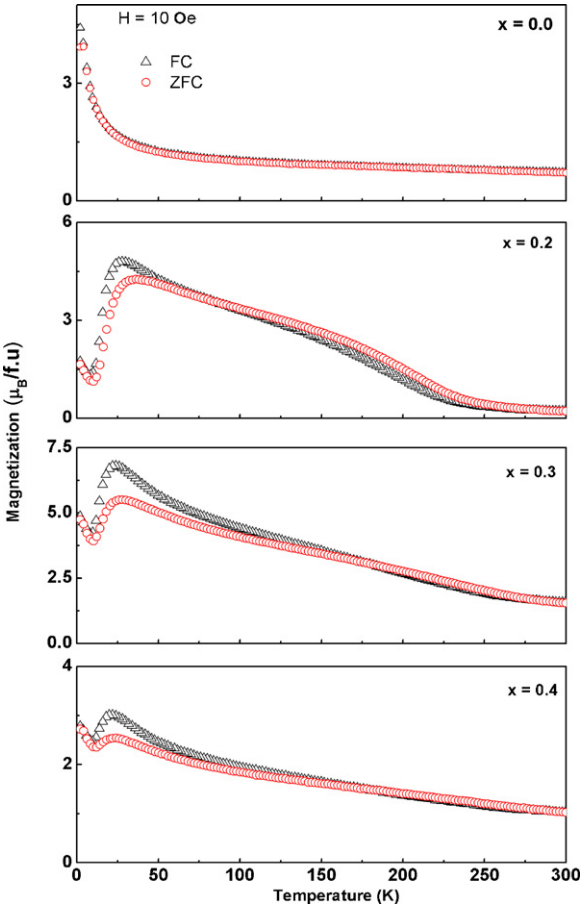


**Fig. 7.** Magnetization vs. temperature plot for $GdFe_{1-x}Ni_xO_3$ ($x = 0.0$, 0.2, 0.3, 0.4) sample in presence of magnetic field of 10 Oe.

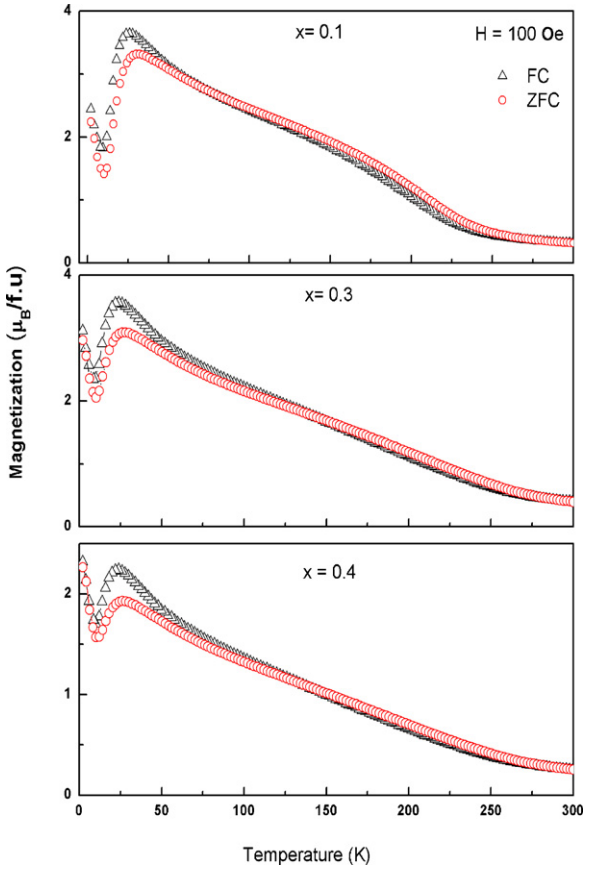


**Fig. 8.** Magnetization vs. temperature plot for $GdFe_{1-x}Ni_xO_3$ ($x = 0.1$, 0.3, 0.4) sample in presence of magnetic field of 100 Oe.

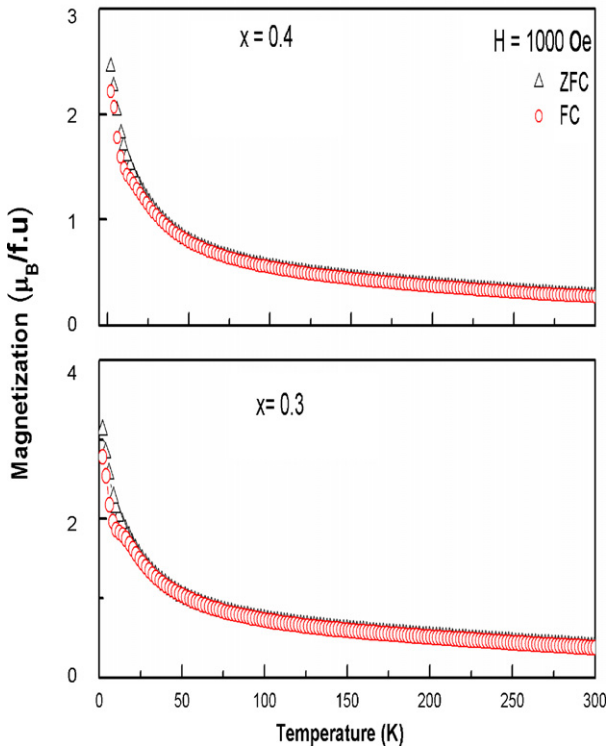


**Fig. 9.** Magnetization vs. temperature plot for $GdFe_{1-x}Ni_xO_3$ ($x = 0.3$, 0.4) sample in presence of magnetic field of 1000 Oe.

showing the dominance of paramagnetic Gd sublattice over the Fe/Ni sublattices.

When the magnetic field is increased up to 100 Oe, i.e., by a factor of 10, the doped samples with 10, 30 and 40% Ni substitution show similar behavior as at 10 Oe with a decremental trend in the magnetic moments. The transition occurs at 25.5 K, 23.5 K and 23.5 K with magnetic moment of 3.65, 3.56 and 2.23 $\mu_B$/fu, respectively. As the temperature is further lowered, the system shows again a transition at 9.50 K, 8.50 K and 8.56 K. having magnetic moments of 1.825, 2.34 and 2.23 $\mu_B$/fu, respectively. At 1000 Oe, the system shows a completely different behavior where the antiferromagnetic interactions of the sublattice get broken and the system shows paramagnetic behavior, and the magnetic moments are 3.12 and 2.44 $\mu_B$/fu for $x = 0.3$ and 0.4, respectively, at 2 K. Such transition is a signature of complex magnetic structure, which indicates the competition between paramagnetic Gd ions and ferromagnetic Fe/Ni ions within the ensemble. While comparing the magnetic behavior of $GdFe_{1-x}Ni_xO_3$ with $SmFe_{1-x}Ni_xO_3$, there is an enhanced magnetic moment. This can be due to the outer configuration of $Gd^{3+}$ ions with $4f^7$, while as for $Sm^{3+}$ it is $4f^5$ [12]. It is pertinent enough to mention that more detailed studies are required to investigate the temperature dependent magnetic behavior of these Ni doped $GdFeO_3$ samples, which can be done through Mossbauer measurements and magnetic measurements.

## 6. Conclusions

Single phase polycrystalline $GdFe_{1-x}Ni_xO_3$ ($0 \le x \le 0.5$) samples were prepared using solid state reaction technique. The XRD analysis shows a decrease in volume with the increase in the Ni concentration, due to smaller ionic radii of Ni than Fe. Analysis of the $GdFe_{1-x}Ni_xO_3$ ($0 \le x \le 0.5$) using the NEXAFS confirms the octahedral symmetry and oxidation state of the Fe, Ni and Nd ions as +3. The impact of hybridization increases between Ni 3d and O 2p orbitals and the very increase of Ni concentration increases the density of states. The dominant paramagnetic contribution of Gd sublattices clearly supported through *M–H* and *M–T* measurements at varied fields clearly indicates the significance of the rare earth sublattice. In a nutshell, the doping of Ni at Fe sites enables tailoring the magnetic properties of the system, showing transition of magnetic properties, which can be implemented in the applications of magnetic devices and hence controlling the carriers and the moments of these systems.

## Acknowledgments

Authors acknowledge the financial support from the Department of Science and Technology (DST), India, for this work under the project no. SR/S2/CMP/0051/2007. The authors are thankful to Dr. P. Thakur for carrying out the X-ray absorption spectroscopy (NEXAFS) experiments performed at the soft X-ray beamline 7B1 XAS KIST of the Pohang Light Source (PLS), Materials Science and Technology Research Division, KIST, Seoul 136-791, South Korea.

## References

[1] M. Imada, A. Fujimori, Y. Tokura, Rev. Mod. Phys. 70 (1998) 1039–1263.
[2] M.W. Lufaso, P.M. Woodward, Acta Crystallogr. B 57 (2001) 725–738.
[3] R.L. White, J. Appl. Phys. 40 (1969) 1061–1069.
[4] R.M. Bozorth, D. Williamsh, E. Walsh, Phys. Rev. 103 (1956) 572–578.
[5] Y. Okimoto, T. Katsufuji, T. Ishikawa, A. Urushibara, T. Arima, Y. Tokura, Phys. Rev. Lett. 75 (1995) 109–112.
[6] D.D. Sarma, N. Shanthi, P. Mahadevan, Phys. Rev. B 54 (1996) 1622–1628.
[7] P. Ganguly, N.Y. Vasanthacharya, C.N.R. Rao, P.P. Edwards, J. Solid State Chem. 54 (1984) 400–406.
[8] A. Chainani, D.D. Sarma, I. Das, E.V. Sampathkumaran, J. Phys. Condens. Matter 8 (1996) L631–L636.
[9] R. Kumar, R.J. Choudhary, M. Wasi Khan, J.P. Srivastava, C.W. Bao, H.M. Tsai, J.W. Chiou, K. Asokan, W.F. Pong, J. Appl. Phys. 97 (2005) 093526–093532.
[10] R. Kumar, R.J. Choudhary, M. Ikram, D.K. Shukla, S. Mollah, P. Thakur, K.H. Chae, B. Angadi, W.K. Choi, J. Appl. Phys. 102 (2007) 073707–073716.
[11] A. Bashir, M. Ikram, R. Kumar, P. Thakur, K.H. Chae, W.K. Choi, V.R. Reddy, J. Phys. Condens. Matter 21 (2009) 325501–325511.
[12] A. Bashir, M. Ikram, R. Kumar, P. Thakur, P.N. Lisboa-Filho, Mater. Sci. Eng. B 172 (2010) 242–247.
[13] A. Bashir, M. Ikram, R. Kumar, J. Magn. Magn. Mater. 322 (2010) 2581–2584.
[14] S. Geller, E. Wood, Acta Crystallogr. 9 (1956) 563–568.
[15] J.R. Carvajal, Physica B & C 192 (1993) 55–69.
[16] F.M.F. de Groot, M. Grioni, J.C. Fuggle, J. Ghizsen, G.A. Sawatzky, H. Petersen, Phys. Rev. B 40 (1989) 5715–5723.
[17] J.H. Guo, L. Vayssieres, C. Persson, R. Ahuja, B. Johansson, J. Nordgren, J. Phys.: Condens. Matter 14 (2002) 6969–6974.
[18] C.L. Dong, C. Persson, L. Vayssieres, A. Augustsson, T. Schmitt, M. Mattesini, R. Ahuja, C.L. Chang, J.-H. Guo, Phys. Rev. B 70 (2004) 195325–195330.
[19] P. Abbamonte, L. Venama, A. Rusydi, G.A. Sawatzky, G. Logvenov, I. Bozovic, Science 297 (2002) 581–584.
[20] Y. Joly, D. Cabaret, H. Renevier, C.R. Natoli, Phys. Rev. Lett. 82 (1999) 2398–2401.
[21] E. Pellegrin, N. Nucker, J. Fink, S.L. Molodtsov, A. Gutierrez, E. Navas, O. Strebel, A. Krol, J.L. Peng, Z.Y. Li, R.L. Greene, Phys. Rev. B 47 (1993) 3354–3367.
[22] T.J. Regan, H. Ohldag, C. Stamm, F. Nolting, J. Luning, J. Stohr, R.L. White, Phys. Rev. B 64 (2001) 214422–214433.
[23] E.U. Condon, G.H. Shortley, The Theory of Atomic Spectra, Cambridge University Press, Cambridge, 1963.
[24] B.T. Thole, G.V. Laan, J.C. Fuggle, G.A. Sawatzky, R.C. Karnatak, J.M. Esteva, Phys. Rev. B 32 (1985) 5107–5118.
[25] C. Bonnelle, R.C. Karnatak, N. Spector, J. Phys. B 10 (1977) 795–801.
[26] G. Kaindl, G. Kalkowski, W.D. Drewer, B. Perscheibl, F. Holtzberg, J. Appl. Phys. 55 (1984) 1910–1916.
[27] G.W. Durbin, C.E. Johnson, M.F. Thomas, J. Phys. C: Solid State Phys. 10 (1977) 1976–1978.
[28] J.D. Cashion, A.H. Cooke, D.M. Martin, M.R. Wells, J. Phys. C: Solid State Phys. 3 (1970) 1612–1620.
[29] V. Bedekar, O.D. Jayakumar, J. Manjanna, A.K. Tyagi, Mater. Lett. 62 (2008) 3793–3795.